Effect of ion implantation on the electronic structure of bismuth

E. M. Kunoff* and M. S. Dresselhaus
Department of Physics, Massachusetts Institute of Technology, Cambridge, Massachusetts 02139

Y. H. Kao
Department of Physics, State University of New York at Stony Brook, Stony Brook, New York 11794-3800
(Received 2 May 1986)

The magnetoreflection technique has been used to determine the effects of isoelectronic implantation on the bismuth electronic structure as a function of various implantation parameters, including fluence and size of implanted species, temperature of sample during implantation, and ion-beam current. Measured changes in the magnetic energy subbands have been related to strains and defects introduced into the crystal lattice by the implantation process. Implantation-induced strains have been shown to be the cause of a decrease in the L-point energy-band gap. A model has been proposed to calculate the strains which are then related to the measured energy gap changes via deformation potential theory. Extended x-ray-absorption fine-structure and Rutherford-backscattering channeling measurements locate the implanted atoms preferentially at substitutional sites for implantation temperatures of $\gtrsim 50$ °C and at interstitial sites for lower temperatures. Interstitials give rise to inversion-symmetry-breaking magneto-optical transitions and a broadening of the resonance linewidth. Observation of a line-shape reversal indicates an increase of the plasma frequency by an order of magnitude for Bi-ion fluences $\gtrsim 2\times 10^{15}$ cm^{-2}.

I. INTRODUCTION

Ion implantation is a physical mechanism that makes possible the introduction of virtually any foreign species into a host material in a controlled manner. By varying the energy of ions of a chosen mass, different depth distributions can be achieved, thereby providing a method for placing a specific concentration of impurities in a desired volume of a solid. While this method has been used extensively to dope semiconductors to make devices,[1] very little work has been done to study the actual effect of implantation on electronic band structure.[2-4] In this paper, we present results of a comprehensive study relating changes in the bismuth electron energy bands to implantation-induced modifications of the lattice structure.

The semimetal bismuth was chosen as the subject of this study for several reasons. First, its band structure near the Fermi level is well understood due to extensive experimental[5-8] and theoretical[9-11] studies. Its extremely small effective mass ensures that the conditions $\omega_c\tau > 1$ and $\hbar\omega_c > kT$ are achieved at attainable fields, the conditions necessary for the observation of magneto-optical resonant effects. This makes the magnetoreflection experiment a powerful tool for probing changes in the bismuth electronic structure induced by ion implantation. This experiment has the further advantage that the skin depth of the infrared radiation used is comparable to the penetration depth of the implanted ions. We therefore have a probe that is sensitive to changes in the electronic bands in the region most directly affected by ion implantation.

In preliminary work,[12] bismuth was implanted with antimony to fluences 2.2×10^{15} cm^{-2} and 5.5×10^{15} cm^{-2}, concentrations which, when introduced by alloying, result in semiconducting behavior. This was expected to create a semiconducting layer near the bismuth surface; magnetoreflection measurements show rather that the number of charged carriers is greatly enhanced and semimetallic behavior is retained. In the present work, a systematic study of the effects of fluence and size of the implanted ions was subsequently carried out, restricting the implanted species to elements isoelectronic to bismuth: arsenic, antimony, and bismuth. This ensured that the electronic structural changes we observe are induced by the implantation process and by the presence in the lattice of implanted ions, as opposed to doping effects of donor or acceptor atoms. Our magnetoreflection measurements, presented in Sec. II, show that the L-point energy gap and electron effective mass decrease as both the fluence and size of the implanted ions are increased.[2,4] In the discussion in Sec. V, we relate this dependence to long-range strains in the lattice using deformation potential theory. The effects of implantation-induced lattice damage on the magnetic energy levels have been studied as a function of sample temperature during implantation. This is included in Sec. II.

The modifications to the bismuth lattice structure were studied using two complementary methods. In Sec. III, results of extended x-ray-absorption fine structure (EXAFS) measurements on bismuth implanted to high doses of arsenic are presented, giving information on the bismuth lattice structure in the immediate vicinity of an implanted arsenic atom. We show that the implanted species come to rest in different lattice positions depending on sample temperature during implantation. This is corroborated by Rutherford-backscattering (RBS) channeling experiments described in Sec. IV, which gave further information about implantation-induced damage to

the lattice. The implications of all these experiments are discussed and related to the bismuth electronic band structure in Sec. V.

II. MAGNETOREFLECTION STUDIES OF ION-IMPLANTED BISMUTH

Magnetoreflection has been shown to be a powerful probe of the electronic structure of bismuth close to the Fermi level in terms of the $\mathbf{k}\cdot\mathbf{p}$ two-band model parameters.[8,13–15] Due to the extremely small effective mass component at the L-point band minimum, $0.00198m_0$, the condition $\omega_c\tau > 1$ is satisfied over a large range of magnetic fields, so that for the field parallel to the binary crystallographic direction, along $(1\bar{1}0)$, electrons easily complete a cyclotron orbit before being scattered so that resonant transitions are observable over a wide variety of experimental conditions. The small effective mass also ensures that $\hbar\omega_c > kT$ for temperatures even up to room temperature;[13] this means that the characteristic magnetic energy $\hbar\omega_c$ is much greater than the thermal energy, allowing good resolution of the Landau levels and, hence, observation of resonant transitions between them. For these reasons, magnetoreflection has been successfully used to measure variations in the bismuth electronic band parameters as a function of temperature,[16] pressure,[17] alloy concentrations,[8,18] and, most recently, fluence of implanted ions.[2,12]

The fact that resonant transitions between Landau levels are observed in ion-implanted bismuth is in itself noteworthy. This indicates that in the volume probed by the incident radiation, there are still significant regions that are sufficiently undamaged for the condition $\omega_c\tau > 1$ to hold. Using the Lindhard-Scharff-Schiøtt (LSS) (Ref. 19) parameters characterizing the profile of implanted ions, the penetration depth R_p, and the Gaussian width ΔR_p, the implanted crystal can be considered as consisting of three regions: the near-surface region R_s, in which the energetic ions cause little damage, the implanted region $R_p-\Delta R_p \lesssim x \lesssim R_p+\Delta R_p$, in which the processes slowing and finally stopping the ions cause the most damage, and the region just beyond the implanted region $R_>$ containing long-range strains to the lattice.[20] The close similarity of the magnetoreflection spectra from ion-implanted bismuth to those from the virgin crystal indicates that the spectra are for the most part due to transitions made by carriers in the regions R_s and $R_>$, as also found in the case of ion-implanted graphite.[3]

Because the L-point energy gap is so small, only 13.8 meV, the energy range of interesting interband transitions is in the infrared, from 4 to 20 μm. These wavelengths have skin depths in bismuth from approximately 1000 to 3000 Å, roughly one to three times the far end of the implanted region, $R_p+\Delta R_p = 773.4$ Å for 150 keV ^{75}As, the principal subject of investigation in this paper and two to six times $R_p+\Delta R_p = 422.2$ Å for 150 keV ^{209}Bi, the heaviest implant studied. Magnetoreflection is therefore very sensitive to the energy-band structure of electrons in the volume of the bismuth crystal most directly affected by the implantation, that containing the implanted species and the strained volume just beyond. Since the ratio of the implanted to probed volumes varies with incident photon energy from $\lesssim 1$ at the shortest wavelengths to approximately $\frac{1}{3}$ at the longest wavelengths used, variation in linewidth and signal-to-noise ratio with incident photon energy yields information determining the volume containing the electrons which make the resonant transitions. In Sec. II B, it is shown that the low-energy magnetoreflection spectra, from which the L-point energy gap is determined, are in fact due to carriers in the region beyond which the implanted species reside; this is the volume containing the strained lattice which is discussed further in Sec. V.

To obtain the electronic energy-band parameter values, curves of incident photon energy versus resonant field position are fit to the expressions[8] for transitions between $j \neq 0$ levels,

$$\hbar\omega = (\varepsilon^2+2\gamma Hj)^{1/2}+[\varepsilon^2+2\gamma H(j+1)]^{1/2} \tag{1}$$

and the four transitions from the nondegenerate $j=0$ level to the $j=1$, $s=\pm\frac{1}{2}$ levels,

$$\hbar\omega = [(\varepsilon - |G_0\beta^*|H)^2+(Q\beta^*H)^2]^{1/2} \pm[(\varepsilon^2+2\gamma H)^{1/2}+2sG\beta^*H]\,, \tag{2}$$

allowing the parameters to vary. These parameters are $\varepsilon = E_g/2$, half the energy gap, and $\gamma = E_g/\beta^*$ which can be expressed in terms of the effective Bohr magneton, $\beta^* = \beta_0 m^*/m_0$ or the square of the intraband momentum matrix element:

$$\gamma = \frac{e\hbar}{2m^2c}\langle c|p|v\rangle\langle v|p|c\rangle\,. \tag{3}$$

G is the effective g factor for the $j\neq 0$ levels and G_0, slightly different, is that for the $j=0$ levels. Q is the parameter introduced by Baraff[21] to account for coupling to other bands. The high-energy, high-field transitions determine γ; the remaining parameters ε, G_0, and Q, are fixed by the low quantum limit $j=0\leftrightarrow 1$ transitions. This procedure is the same as that used to analyze magnetoreflection spectra taken from bismuth alloys[13,17,18] and bismuth under pressure.[17] It was due to these successful magnetoreflection experiments that this project was launched; ion implantation, like alloying, introduces foreign species into the crystal which, due to the nature of implantation, exert a "negative" pressure on the lattice causing a lattice expansion.

In addition to determining the energy-band parameters, analysis of magnetoreflection spectra gives valuable information concerning lattice damage and symmetry. In magnetoreflection studies of tin-doped bismuth,[18] two classes of Landau-level transition series were observed that do not occur for pure bismuth. It was found that one of these corresponded to transitions forbidden by the selection rules dictated by the inversion symmetry of the bismuth lattice. The resonances were fit very well as $\Delta j=0$ and $\Delta j=\pm 2$ transitions. The resonances of the second series were manifest only at low energy and, in fact, became the dominant features in the spectrum at the lowest energies. These were attributed to transitions between impurity-perturbed Landau levels. As the transi-

tion energy increases, the resonant field does likewise, so that the radius of the cyclotron orbit, which is inversely proportional to H, becomes smaller. At high enough fields, the cyclotron radius becomes smaller than the average separation between impurities, excluding them from the electron's orbit, so that the electron then reverts to the cyclotron motion more similar to that of pure bismuth.

The width of the resonant transitions, ΔH, also gives information concerning the amount of damage to the crystal. Since $\Delta H/H \sim (\omega_c \tau)^{-1}$, the slopes of plots of H versus ΔH for different samples give the relative values of relaxation time τ and proportional to it, the mean-free path of an electron. This analysis is made for all samples to obtain the dependence of mean-free path on fluence, sample temperature during implantation, and ion-beam current.

The magnetoreflection experimental setup and sample preparation are described in Sec. II A. Experimental results are presented in the three Secs. II B—II D. In the first, Sec. II B, the line shape of the resonances is described. It was found that for implantation to high fluence or with large ions, the resonant positions are shifted from the reflectivity maxima in the pure bismuth spectra to the reflectivity minima, indicating an increase of the plasma frequency from $\hbar\omega_p = 30.9$ meV which is below our lowest incident photon energy, to a value greater than our highest incident energy 300 meV. Because the identification of the resonance point within the linewidth affects all subsequent analysis of the spectra, Sec. II B is devoted to an explanation of resonance classifications.

Section II C consists of results from samples implanted at room temperature. The magnetoreflection spectra are compared to those of pure bismuth to point out the changes induced in the band structure of the implanted samples. The variation of the energy-band parameters with the fluence and the size of the implanted species is given. Further analysis of these trends is relegated to Sec. V, incorporating results of EXAFS and RBS-channeling measurements.

Section II D consists mainly of magnetoreflection results for samples implanted at low temperature, focusing on the information pertaining to lattice damage contained in the spectra. Comparison is made to the magnetoreflection spectra of tin-doped bismuth[18] for which forbidden and impurity-level transitions were observed. Low-temperature implantation was done at two different current densities and the effect of this implantation variable on lattice damage and strain is studied as well.

A. Experimental details

The magnetoreflection experiments were done on two sets of samples that were chosen to study the two principal effects of isoelectronic implantation, namely, lattice strain and lattice damage. Samples used were cut with a string saw from a bismuth single crystal oriented in the binary direction. The surfaces of the $5\times10\times1$ mm^3 slabs were prepared as described elsewhere.[2,20] Those comprising the first set were implanted at room temperature with three species isoelectronic to bismuth: arsenic, antimony, and bismuth itself, to determine the change in electronic band parameters as a function of implant size. These were all implanted at 150 keV with low current density, $\lesssim 10$ μA, to one of three different fluences: 2.2×10^{15}, 5.5×10^{15}, or 1.0×10^{16} cm^{-2}, to study the dependence of band parameters on the implant concentration.

The second set were all cooled to different temperatures during implantation with ^{75}As at 150 keV to a fluence of 1.0×10^{16} cm^{-2}, which, for the room-temperature case, exhibited extremely smooth magnetoreflection traces despite large changes in the band parameters. During implantation, the samples were cooled by contact with a copper cold finger containing liquid N_2, a dry ice-isopropyl alcohol mixture or icewater. Temperatures, measured with a thermocouple next to the sample, averaged 83, 250, and 298 K, respectively, for the three samples. The cooled samples were implanted with beam current in one of two regimes: $\lesssim 10$ μA or $\gtrsim 40$ μA. Magnetoreflection measurements on these samples gave information concerning implantation-induced lattice damage as well as lattice strain, complementary to both the earlier magnetoreflection studies and the EXAFS and RBS-channeling results presented in Secs. III and IV, respectively.

The magnetoreflection experimental setup has been described in detail elsewhere[20] and has been used in most of the previous studies of bismuth and bismuth alloys mentioned in this work.[2,8,12,13,16,18] The samples were attached with silver paint to a copper cold finger in a dewar cooled with liquid helium, placed in the center of the 2-in. bore of a 15 T Bitter solenoid at the Francis Bitter National Magnet Laboratory. Magnetoreflection measurements were made in the Faraday geometry, the magnetic field parallel to the incident radiation normal to the sample surface. The infrared radiation was provided by a globar. Photon energies were selected in the range $85 < \hbar\omega_c < 300$ meV using a single-pass monochromator.

B. Resonance line shapes

In the first magnetoreflection studies of ion-implanted bismuth,[12] it was observed that the reflectivity minima were much sharper than the maxima which give the resonant field positions of the Landau-level transitions for pure bismuth.[14] This effect is seen in Fig. 1 in which both traces were taken at incident photon energy 200 meV, the top from a pristine bismuth sample and the lower from a bismuth sample implanted with antimony to a fluence of 5.5×10^{15} cm^{-2}. In addition to the narrowing of the minima, it is seen that the left side of the minimum of the ion-implanted sample is convex as opposed to that of the bismuth sample which is concave. We note also that in the spectrum from the pristine bismuth sample, most of the noise in the trace occurs near the minimum; the opposite is the case in the implanted bismuth spectrum. Based on these deviations from the pure bismuth line shape, resonances were identified with the minima in the spectra as would be expected from an increase in the plasma frequency for the implanted sample.

Further support for this identification was obtained when taking spectra from a bismuth sample implanted with a lighter species, arsenic. At the lowest fluence stud-

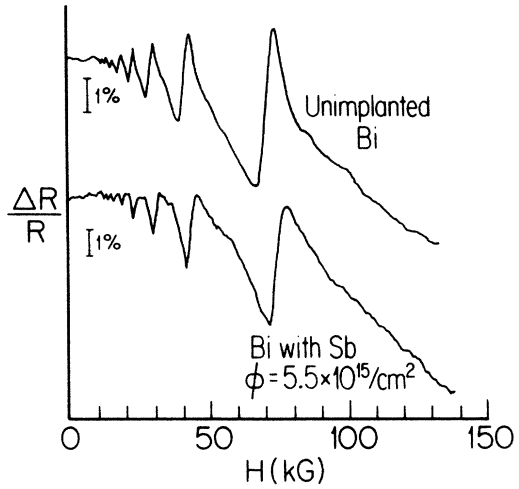

FIG. 1. Comparison of magnetoreflection resonant line shapes between spectra taken at 200-meV incident photon energy from a pristine bismuth sample and a sample implanted with antimony to a fluence of 5.5×10^{15} cm^{-2}. The sharpening of the reflectivity minima, increased noise near the maxima and convexity on the low-field side of the minima in the implanted sample all help to identify the reflectivity minima with the resonant transitions in the implanted sample.

ied, 2.2×10^{15} cm^{-2}, no change in line shape was observed; at the highest fluence, 1.0×10^{16} cm^{-2}, a line shape similar to that for antimony implantation was obtained. This is seen in Fig. 2 which consists of magnetoreflection traces taken at incident photon energy 200

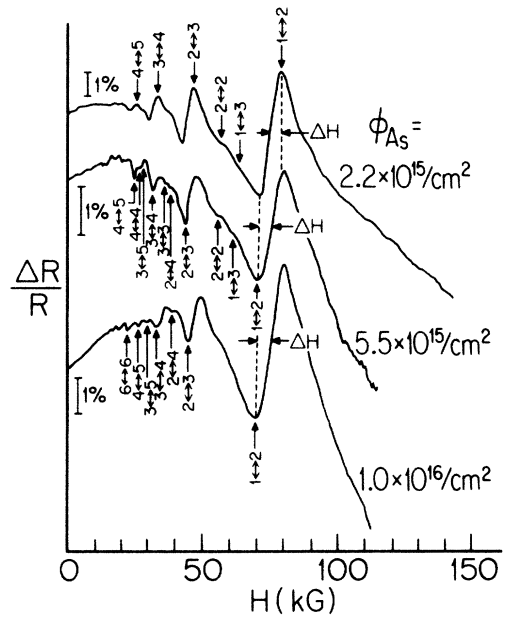

FIG. 2. Experimental magnetoreflection traces showing the effect of fluence on the spectra. All spectra were taken at photon energy 200 meV for bismuth implanted with arsenic. The fluences shown are 2.2×10^{15} cm^{-2} (top), 5.5×10^{15} cm^{-2} (middle), and 1.0×10^{16} cm^{-2} (bottom). Resonant transitions are labeled by $j\leftrightarrow j'$ as discussed in the text. Horizontal lines indicate the $j=1\leftrightarrow2$ linewidths ΔH.

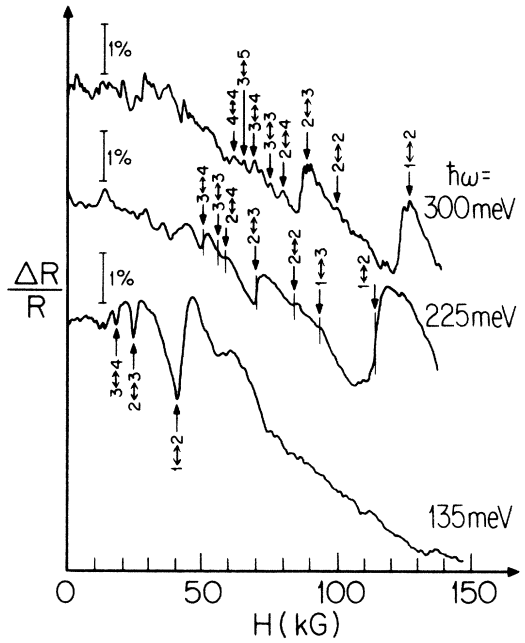

FIG. 3. Effect of photon energy on the magnetoreflection traces for the binary face of bismuth implanted with As to a fluence of 5.5×10^{15} cm^{-2}. The magnetoreflection traces were taken at energies 300, 225, and 135 meV from top to bottom, respectively, exhibiting line-shape reversal as the photon energy moves through $\hbar\omega_p$.

meV for these two samples and a third, implanted with arsenic to a fluence of 5.5×10^{15} cm^{-2}, which also exhibits resonances at the reflectivity minima at this incident photon energy. The line shapes were also found to depend on photon energy, as seen in Fig. 3. In Figs. 2 and 3, the resonant magnetic fields used in the analysis of the experimental results are indicated by arrows.

As mentioned above, the line-shape reversal indicates that the plasma frequency is higher than the frequency of the incident photon. For the higher fluence arsenic-implanted samples and the heavier mass antimony and bismuth-implanted samples, resonant transitions occurred at the reflectivity minima in the spectra taken over the entire range of photon energies used, from 90 to 300 meV, indicating that $\hbar\omega_p > 300$ meV for these samples. In the sample implanted with arsenic to a fluence of 5.5×10^{15} cm^{-2}, however, we observe the reversal of line shape at an energy within our range of incident energies; this is seen in the center trace of Fig. 3, taken at incident photon energy 225 meV. Based on the plot of photon energy versus resonant magnetic field, called a fan chart (see Fig. 4), we identified the resonance at this energy with the inflection point. For higher photon energies, the resonances were located at the reflectivity maxima, as in pure bismuth, while at lower energies they were taken at the minima. This was the only identification that would give us the smooth curves that could be fit to the magnetic energy levels as given in Eqs. (1) and (2). The fit using this identification transitions is shown in Fig. 4(b).

The increase of the plasma frequency by an order of magnitude for the high fluence arsenic-implanted samples

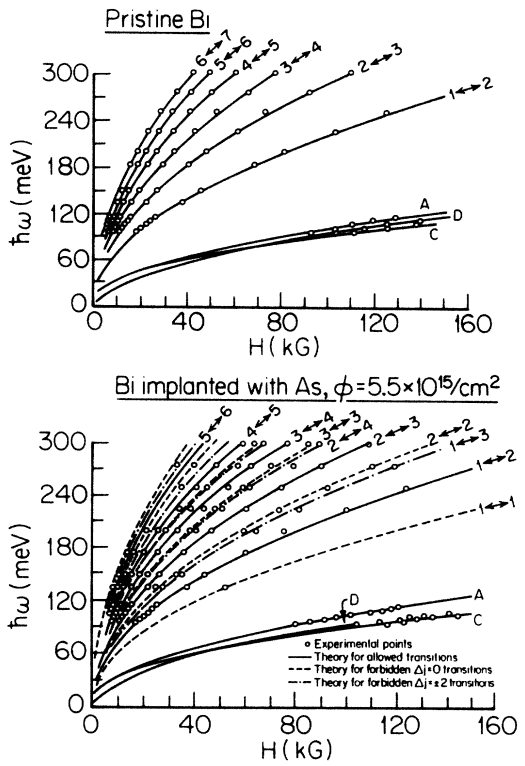

FIG. 4. Plot of photon energy vs resonant magnetic field for (a) pristine bismuth and (b) bismuth implanted with As to a fluence of 5.5×10^{15} cm^{-2}.

and for the antimony and bismuth-implanted samples studied here implies a change by two orders of magnitude in the number of carriers, assuming the static dielectric constant remains essentially unchanged, since

$$\omega_p^2=\frac{4\pi Ne^2}{m^*\epsilon_0}\ . \tag{4}$$

We expect little change in the dielectric constant, ϵ_0, because its large anisotropy, $\epsilon_0^{\parallel}\approx30$ parallel to the trigonal direction and $\epsilon_0^{\perp}\approx100$ in the plane perpendicular to it, is due to the large anisotropy in the effective-mass components[22] which we find do not change significantly upon implantation. The small decrease found for m^* in this work is much too small to account for the huge change in the plasma frequency. If increased carrier concentration is the major effect causing the increase in the plasma frequency, then the necessary increase by a factor of 100 implies a significant increase of the L- to T-point band overlap, 38.5 meV in pure bismuth.[17] As in the work of Boyle and Brailsford,[22] we assume an ellipsoidal pocket at T containing a number of holes equal to the number of electrons contained by the ellipsoids at the three L points. For ellipsoidal bands, $n\sim E^{3/2}$, resulting in an upshift of the T band by 196 meV and downshift at L by 270 meV. While this shift is very large compared to the L-point energy gap of 13.9 meV and the band overlap of 39.5 meV, it is still considerably smaller than the energy difference to the next higher band at the T point. In the work of Golin[23] this separation is calculated to be ~544 meV, so no band crossing is caused, leaving the band structure qualitatively the same. A more direct measurement of the band overlap can be studied through absolute reflectivity measurements or the Shubnikov–de Haas effect.

The arguments given above for determination of resonant field positions are valid for transitions not involving the $j=0$ levels. It has been noted that in the low-energy, high magnetic field regime, an anomalous set of resonances are observed in the magnetoreflection spectra from pure bismuth.[8] These are shown in Fig. 5(a), a trace taken from a pure bismuth sample with incident photon energy 105 meV. Based on a calculation of the line shape using the Baraff Hamiltonian,[21] these resonances were identified as labeled A, C, and D in Figs. 5(a)–(c). Due to the basic similarity of the resonances ob-

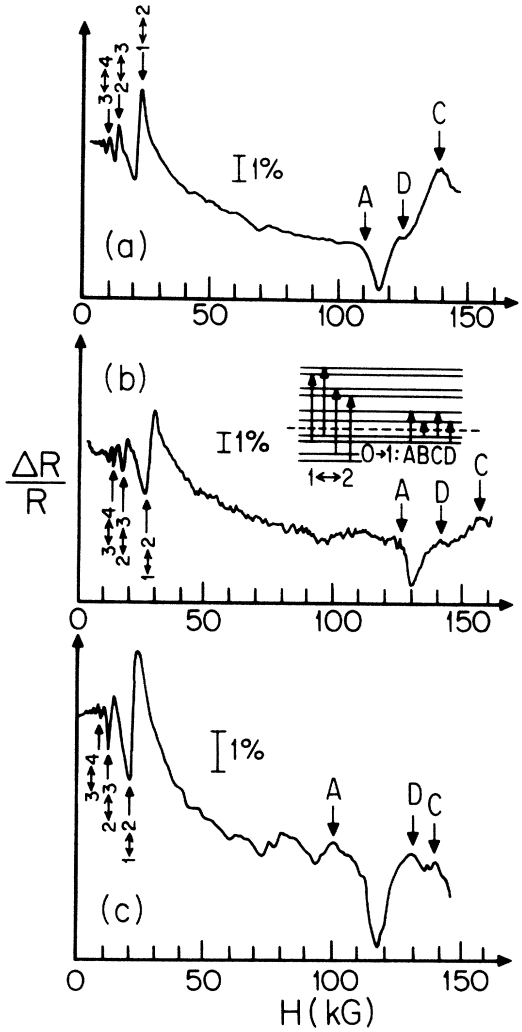

FIG. 5. Experimental magnetoreflection traces taken at photon energy 105 meV for (a) pristine bismuth, (b) bismuth implanted with Sb to a fluence of 5.5×10^{15} cm^{-2}, and (c) bismuth implanted with As to fluence 1.0×10^{16} cm^{-2}. Low-field resonances are main series $j\leftrightarrow j+1$ transitions; the higher field resonances, marked A, C, and D are $0\leftarrow1$ low quantum number limit transitions (see inset).

tained in the implanted samples, as seen in Figs. 5(b) and (c) for spectra taken at the same incident photon energy from samples implanted with antimony to fluences of 5.5×10^{15} cm^{-2} and 1.0×10^{16} cm^{-2}, respectively, identification of the resonances was made for the implanted samples in the same way as for pristine bismuth.

C. Room-temperature implanted bismuth

For a given sample, the magnetoreflection spectra can be classified as belonging to one of two regimes: the high-energy regime, exhibiting transitions between $j\neq0$ levels, and the high magnetic field low-energy regime, in which the $0\leftrightarrow1$ transitions are observed. The change of line shape as a function of fluence of implanted ion is shown in Fig. 2, consisting of spectra taken at 200 meV from bismuth samples implanted with arsenic to a fluence of 2.2×10^{15} cm^{-2}, 5.5×10^{15} cm^{-2}, and 1.0×10^{16} cm^{-2}. Each trace in the figure reflects a different aspect of the modifications induced in bismuth by ion implantation.

First, the fluence dependence of the resonant magnetic field value for a Landau-level transition is considered. Following each $j\leftrightarrow j+1$ transition as a function of fluence, a small decrease in the field position of each resonance is observed. The same trend is observed as the size of the implanted ions is increased. The consequence of this shift on the electron energy bands is easily appreciated by looking at Eq. (1), giving the photon energy as a function of resonant field for a $j\leftrightarrow j+1$ transition. For a giving photon energy, a decrease in H for high photon energy results in an increase in the band parameter γ since $\varepsilon\ll\hbar\omega$. In practice, we obtain the implantation-induced modification of all the band parameters by making a least-squares fit of all photon energies as functions of the resonant field positions to both Eqs. (1) and (2) for all transitions from levels j. This produces a fan chart such as those in Fig. 4, derived from the resonances in all the spectra from (a) pristine bismuth and (b) a bismuth sample implanted with arsenic to a fluence of 5.5×10^{15} cm^{-2}.

A second prominent feature distinguishing the traces obtained for implanted samples from those due to pristine bismuth is the appearance of additional transitions. Like the "satellite" s_j resonances observed in the magnetoreflection spectra of tin-doped bismuth,[18] these are identified as transitions forbidden by the inversion symmetry of the bismuth lattice, for which $\Delta j=0,\pm2$; they are labeled thus in Fig. 2. Using the same band parameters that are used to fit the allowed transitions, they are fit by Eq. (1) with the modification that $j+1$ becomes $j+\Delta j$. The curves in the fan chart of Fig. 4(b) not seen in Fig. 4(a) correspond to these forbidden transitions. The presence of these transitions indicates that there are defects in the lattice, most likely interstitials, which break the inversion symmetry.

Again concentrating on Fig. 2, one observes a broadening on the linewidths with increased fluence; the same effect is obtained with larger ion size.[2] A linear least-squares fit of linewidth as a function of resonant field position ΔH versus H has been made for all of the samples discussed in this section.[20] For samples cut from the same crystal, the slopes are found to increase with greater fluences and sizes of the implanted ions. As noted above, the slopes of these lines are inversely proportional to $\omega_c\tau$. Hence, the greater the slope, the shorter the mean-free path, consistent with the presence of lattice defects. One expects that the temperature of the sample during implantation would strongly affect both the linewidth and the presence of forbidden transition; this matter is discussed in Sec. II D.

In calculating the theoretical curves of the fan charts, the four band parameters γ, ε, G_0, and Q, described in Sec. I, are allowed to vary. As already noted, the value of γ is determined by the high-energy $j\neq0$ transitions; the downward shift in resonant field of each transition with increasing fluence and size of implanted ion causes γ to increase slightly. We emphasize the word slightly; the largest change in γ that we obtain is only about 7% as displayed in the graph of Fig. 6. This figure shows clearly that the modification of γ as a function of fluence is much greater for the lighter implant ^{75}As than the heavier ^{209}Bi. In both cases, the lines must converge to the pristine bismuth value for γ, indicated by the dashed line in the figure. Since γ is inversely proportional to the effective mass, it measures the curvature of the bands at the L edge and the strength of the interaction between the valence and conduction bands. Since the larger implanted bismuth atoms cause a greater strain on the lattice than the same fluence of arsenic atoms, this phenomenon cannot be explained in terms of lattice strain by interstitials. If however, the implanted species come to rest at substitutional sites, a smaller implanted atom, differing more in size from a bismuth atom of the pristine lattice, will strain it more than the substitution of an atom closer in size to bismuth. Thus, in the implanted region, one expects a larger change in the momentum matrix element caused by a change in the L-edge wave function for bismuth implanted with arsenic if the implanted atoms are at substitutional sites. Since γ is proportional to the

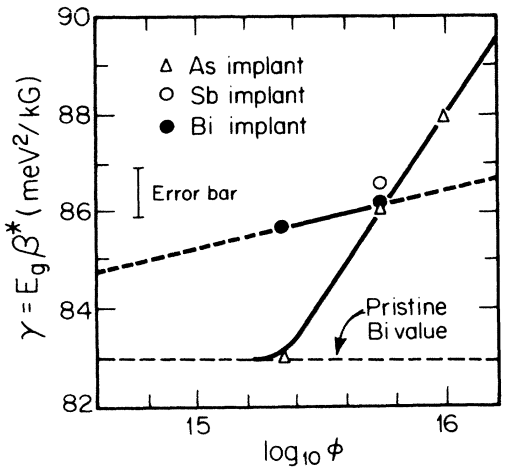

FIG. 6. Plot of γ vs the log of the fluence for bismuth implanted with As, Sb, and Bi. The dashed line indicates the γ value for unimplanted bismuth. The lines through the experimental points are drawn as a guide to the eye.

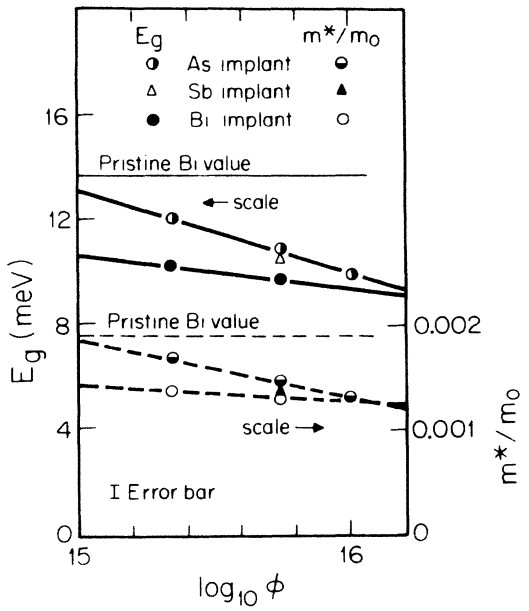

FIG. 7. Upper curves give the dependence of E_g on the log of the fluence for bismuth implanted with As, Sb, and Bi. Below is the log fluence dependence of the effective mass $m^*/m_0=\beta_0 E_g/\gamma$. The lightweight solid and dashed lines indicate the values of E_g and m^*/m_0 for unimplanted bismuth. The lines through the experimental points are drawn as a guide to the eye.

matrix element, a substitutional site for implanted species could explain its functional dependence on ion size. This question is considered again in Sec. II D when the modification of γ as a function of implantation temperature is discussed.

The remaining three parameters characterize the $j=0$ Landau level and are therefore fixed by the 0←1 transitions, observable only at low energy and high magnetic field. Falling on a curve in the fan chart somewhat separated from the $j\neq 0$ level transitions, the $j=0$ transitions are labeled *A*, *C*, and *D* in Fig. 5. The magnetoreflection spectrum in Fig. 5(c), taken in the low-energy regime with incident radiation of energy 105 meV on bismuth implanted with arsenic to a fluence of 1.0×10^{16} cm^{-2} illustrates changes observed in the 0←1 transitions. In addition to the shift of resonant field for each of these transitions, there is a marked change in their relative intensities. Specifically, the interband transition *D*, forbidden in the strict two-band model but made possible by mixing of the $j=0$ levels, becomes greatly enhanced compared to the other two transitions. This is indicative of strong interband coupling between the four 0←1 transitions,[24] made possible by a decrease of the energy gap and an increase in the coupling parameter Q, which is exactly what is obtained by a fit of the resonant fields and energies to the theory of Eqs. (1) and (2). A decrease in the parameter G_0 is also obtained from the fit. The dependence of E_g on fluence and ion size is shown in Fig. 7, along with that of m^*, derived using the relation

$$m^*=E_g\beta_0 m/\gamma\ , \tag{5}$$

where $\beta_0=e\hbar/mc$ is two times the Bohr magneton. In this figure, as in Fig. 6, the dashed and lightweight lines indicate the parameter values for unimplanted bismuth. The values of the band parameters for all the samples discussed in this section are given in Table I.

D. Bismuth implanted at low temperatures

Figure 8 shows typical high-energy regime magnetoreflection traces taken at $\hbar\omega=200$ meV for samples implanted to a fluence of 1.0×10^{16} cm^{-2} but cooled to different temperatures during implantation. The top trace, taken from a sample implanted at room temperature, is very smooth, as is characteristic of traces taken from all samples implanted at room temperature. The next trace down, from a sample that was cooled with dry ice during implantation, is somewhat more noisy, but still exhibits sharp resonances. The resonances in the third trace down, taken from a sample cooled with liquid nitrogen during implantation, are broader. Here the forbidden $\Delta j=0,\pm2$ transitions are stronger and the trace is noiser in general. It should be noted that the samples used for the middle two traces were implanted with a higher beam current $i_b\gtrsim 40$ μA than those used for the other two, the room temperature and a second liquid-nitrogen-cooled sample, for which $i_b\lesssim 10$ μA. The traces taken from the fourth sample cooled with liquid nitrogen during implantation were somewhat anomalous, as is discussed in detail below. The most unexpected feature of this trace is the fact that the resonances are at reflectivity maxima as opposed to the reflectivity minima observed in all other high fluence

TABLE I. Electronic band parameters for ion-implanted bismuth.

Implant	Fluence ($\times10^{15}$ cm^{-2})	γ (meV^2/kG)	E_g (meV)	m^*/m_0 ($\times10^{-5}$)	G ($\times10^{-5}$)	Q ($\times10^{-5}$)	$\hbar\omega_p$ (meV)
None	0.0	83.0	13.8	192	756	252	30.9[a]
As	2.2	83.0	12.0	167	708	391	<95
	5.5	86.1	10.8	145	796	353	~225
	10.0	88.1	9.9	130	834	214	>300
Sb	5.5	86.6	10.6	146	774	29	>300
Bi	2.2	85.7	10.2	137	755	253	>300
	5.5	86.2	9.7	131	755	240	>300

[a]From the work of Boyle and Brailsford (Ref. 22).

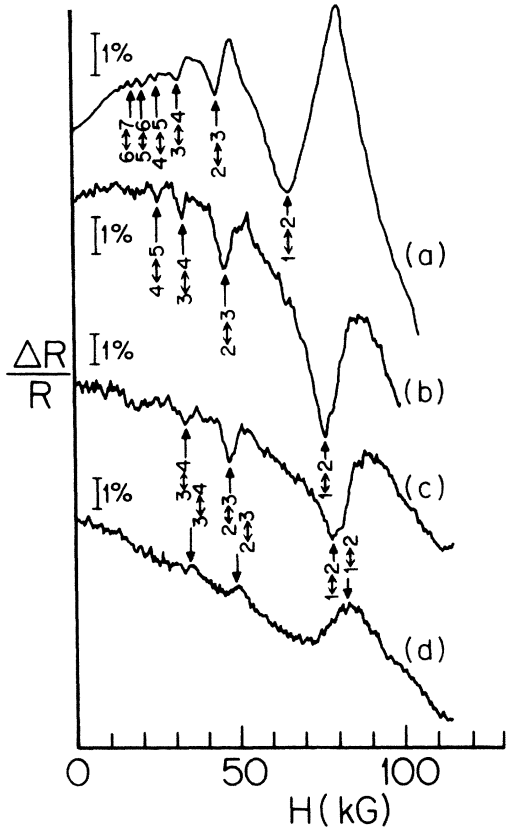

FIG. 8. Magnetoreflection spectra taken at 200 meV from bismuth samples implanted with As to a fluence of 1.0×10^{16} cm^{-2} under the following conditions, from top to bottom: (a) room temperature, low current; (b) dry ice cooled, high current; (c) liquid nitrogen cooled, high current; (d) liquid nitrogen cooled, low current.

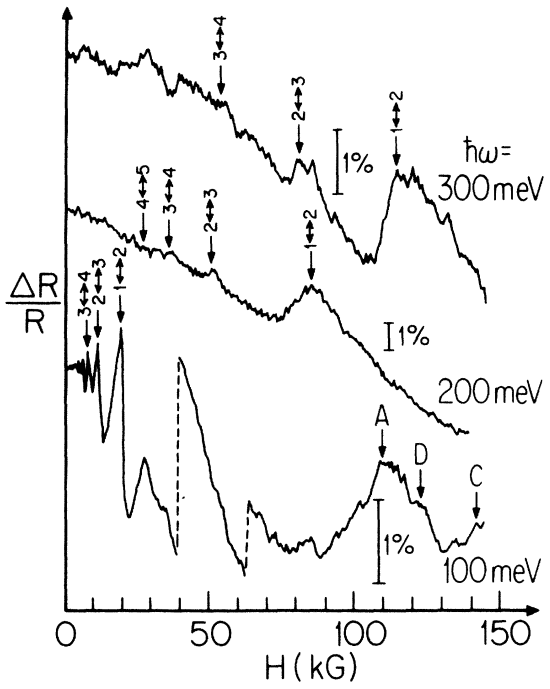

FIG. 9. Magnetoreflection spectra taken from bismuth cooled with liquid nitrogen during low current implantation to a fluence of 1.0×10^{16} cm^{-2} at energies, from top to bottom, of 300, 200, and 100 meV, respectively. Dashed lines indicate that the trace has been cut and displaced vertically upward to fit the entire spectrum into the space of the figure.

implanted samples. In addition, this trace has the smallest signal-to-noise ratio; it is expected, based on reviews of studies of implantation-induced damage in metals,[20,25] that a sample implanted with a smaller beam current is less damaged than one implanted at higher current, all other conditions being the same. Another significant feature of these traces is that as the sample temperature during implantation decreases, the resonance position for a given transition is shifted to higher fields. This pertains to all four samples, since a sample implanted with a lower beam current is heated less by the implantation process. The upshift in magnetic field of the resonant transitions for a given energy from the room-temperature implanted position results in a decrease in the parameter γ, as seen in Table II. This parameter can be directly related by Eq. (3) to the momentum matrix element between the conduction c and valence v bands,[18] so that the change of γ with implantation temperature is related to the change in momentum matrix elements between the valence and conduction bands. As noted by Misu *et al.*,[18] this can be explained by coupling to bands outside the two-band model.

Figure 9 displays one of the anomalous effects observed in the low current liquid-nitrogen-cooled implanted sample mentioned above: the dramatic reduction of noise from the high to lower photon energy traces. In this figure, traces taken from this sample at three different photon energies are shown; in the top trace $\hbar\omega = 300$ meV, in the center 200 meV, and the bottom 100 meV. The signal-to-noise ratio is seen to greatly improve as the photon energy decreases, until, at the lowest energies, the quality of the traces is comparable to those obtained in samples implanted at room temperature. In addition, the slopes of the ΔH versus H plots[20] increase with higher photon energies, also indicating a stronger influence of

TABLE II. Electronic structure parameters for bismuth implanted with arsenic to a fluence of 1.0×10^{16} cm^{-2} at different average implantation temperatures T_i.

T_i (°K)	γ (meV^2/kG)	E_g (meV)	G ($\times10^{-5}$)	Q ($\times10^{-5}$)	$\hbar\omega_p$ (meV)
308	88.1	9.9	834	214	>300
243	86.7	10.4	756	131	>300
117	84.5	10.6	749	134	>300
87	81.0	10.6	931	5	<85

TABLE III. Optical skin depths δ for infrared radiation of selected energies in the range of the magnetoreflection experiment and fraction of crystal in the skin depth δ that contains implants.

$\hbar\omega$ (meV)	δ (Å)	Fraction with ^{75}As
300	1203	0.64
200	1798	0.43
100	3560	0.22

lattice damage in the higher photon energy spectra. This phenomenon can be explained very simply by a comparison of the skin depth of the incident radiation to the ion penetration depth R_p and range scatter ΔR_p. We use the classical expression[26] to calculate the skin depth δ for radiation of frequency ω,

$$\delta = \frac{c}{\sqrt{2\pi\omega\sigma}} , \tag{6}$$

where the conductivity σ is taken from the work of Maltz.[14] The results of this calculation are given in Table III. It is found that for high photon energy, the light penetrates only approximately 1.5 times the thickness of the implanted region, in which most of the lattice damage is contained. As $\hbar\omega$ decreases, the skin depth becomes longer so that the fraction of damaged crystal affecting the measured reflectivity correspondingly decreases.

A second effect is observed in the sample cooled with liquid nitrogen during low current arsenic implantation that is not seen in any of the other implanted samples; this is the appearance of the transition labeled a_1 and a_2 in Fig. 10. These are only present in the low photon energy, low magnetic field range and, as seen in this figure, become stronger, the lower the energy and field, until, at the lowest energies attainable, they become the dominant features of the spectra. The line shapes of these resonances are very distinct from all others in the spectra; in addition to their anomalous growth with decreasing magnetic field, they are more symmetric than the other peaks. Qualitatively, they are the same as the a_j resonances observed in the magnetoreflection spectra of tin-doped bismuth.[18] In that paper,[18] the resonances were identified as transitions between the Landau levels of the cyclotron motions of electrons under an impurity potential described by a linear combination of wave functions for the two nonprincipal L points. As the magnetic field increases, the cyclotron radius decreases until, for some H field, the radius becomes smaller than the average separation between impurities and the electronic orbit no longer contains an impurity. The electrons therefore revert back to the normal cyclotron motion similar to that in pure bismuth and the other implanted samples.

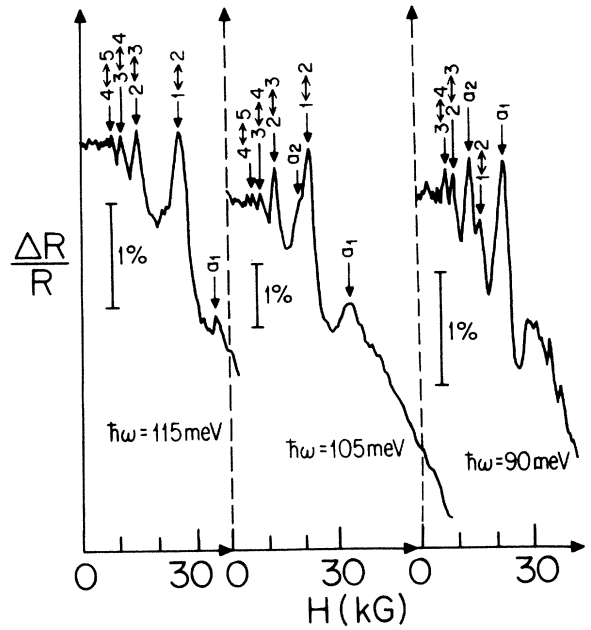

FIG. 10. Magnetoreflection spectra taken at energies, from left to right, of 115, 105, and 90 meV from a bismuth sample cooled with liquid nitrogen during low current implantation to a fluence of 1.0×10^{16} cm^{-2}. The transitions a_1 and a_2 are discussed in the text.

To determine the band parameters of the impurity levels, Misu *et al.*[18] assumed that the impurity-perturbed Landau levels are of the bismuth type and that the a_1 and a_2 lines are the $1\leftrightarrow2$ and $2\leftrightarrow3$ transitions, respectively. The parameters ε and γ were than obtained by a least-squares fit, yielding the values $\varepsilon=24$ meV and $\gamma=44$ meV^2/kG. Applying the same method to our series of transitions gives $\varepsilon=21.7$ meV and $\gamma=50.6$ meV^2/kG, roughly similar values.

The observation of these transitions and the fact that they can be fit as impurity-perturbed Landau-level transitions using similar parameters to those found for the tin alloy only in the sample implanted at low temperature with low current implies that this sample is the most like the tin-doped sample; arsenic impurities have a concentration similar to the tin concentration in the volume probed by the infrared radiation. This implies that, in the samples implanted at room temperature, the arsenic diffused further into the sample, making the impurity concentration too low to be observed in the attainable low-energy low-field region. In the case of the samples implanted at low temperature with high current, more damage was created in the volume containing the arsenic, so that complete orbits containing an arsenic impurity are not possible.

To summarize, we find that lowering the sample temperature during implantation to a given fluence has only a small effect on the energy gap and $j=0$ band parameters, as opposed to γ which decreases measurably. This implies a decrease in the momentum matrix elements which can be due to coupling with bands outside the two-band model. Second, in samples implanted at low temperature with low current, the diffusion of implanted species is curtailed and lattice damage is mainly restricted to the region between the surface and $R_p+\Delta R_p$, as supported by the improved quality of magnetoreflection spectra with lower photon energies and the identification of anomalous resonances with the impurity-perturbed Landau-level transitions observed in tin-doped bismuth.[18] The magnetoreflection spectra of samples implanted at low tempera-

ture further imply that diffusion of implanted species occurs in samples implanted at room temperature.

III. EXAFS STUDIES OF ARSENIC-IMPLANTED BISMUTH

Measurement of the (EXAFS) extended x-ray-absorption fine structure has been shown to be a powerful tool for studying the local structure of a crystalline or amorphous solid.[27] In particular, analysis of the fluorescence EXAFS from arsenic implanted in silicon[28] and bismuth[4,20] has yielded much information about these materials. In this section, we present results of EXAFS measurements for the fluorescence of arsenic atoms implanted into bismuth at different temperatures. Section II A consists of details of sample preparation and the experimental setup and Sec. II B contains the experimental results and analysis.

A. Experimental details

Bismuth slabs were cut and polished in the same manner as those used for the magnetoreflection experiments described in the last section. During implantation, they were cooled with either liquid-nitrogen vapor (sample LNV) to ~ 250 K or liquid nitrogen (sample LN) to ~ 83 K. To maximize the number of arsenic atoms excited by x rays incident at glancing angles, the samples were implanted at succeeding beam energies 200, 100, 40 keV to fluences 2.5×10^{16} cm^{-2}, 1.25×10^{16} cm^{-2}, and 1.25×10^{16} cm^{-2}, respectively. This resulted in an approximately constant arsenic concentration extending from the sample surface to a depth of 625 Å as calculated by LSS theory[19] and as summarized in Table IV.

All EXAFS measurements were made at the Cornell High Energy Synchrotron Source (CHESS) on one of the two C-beam lines. To measure the fluorescence spectra, the ion-implanted samples were placed vertically with the implanted binary face at a glancing angle to the beam. Samples were mounted with vacuum grease on a sample holder designed to allow small changes in the angle between the x-ray beam and the sample holder, up to $\sim 15°$. These were necessary to move Bragg scattering peaks of the bismuth crystal out of our energy range of investigation. A Soller slit assembly[29] with germanium filters was placed normal to the sample to reduce the background scatter. The slit assembly consists of x-ray opaque thin strips whose planes intercept at the sample surface, 1 in. away. Such a configuration does not appreciably attenuate the fluorescence signal from the sample, but the solid angle accessible to the filter fluorescent signal is greatly reduced. The filter has been chosen as a material whose K edge at 11.104 keV lies above the Bi $L\alpha$ line at 10.842 keV, but below the region in which spectra are taken, $11.6 < E < 12.6$ keV, thus sharply attenuating the signal from bismuth scatterers. A scintillation counter, placed immediately following the slit assembly, was used to measure the fluorescence signal.

TABLE IV. Energies and doses for ^{75}As implanted samples used for EXAFS and RBS-channeling measurements.

Energy (keV)	Fluence ($\times10^{15}$ cm^{-2})	R_p (Å)	ΔR_p (Å)
40	1.25	166.39	89.04
100	1.25	343.99	203.2
200	2.50	623.64	371.1

B. Experimental results and analysis

The raw data taken from samples LN and LNV has been presented elsewhere.[4,20] In both spectra, the EXAFS oscillations are evident with very different oscillation frequencies. These fluorescence spectra were converted to a function of wave number and the smooth background absorption was removed using a cubic spline. The data are multiplied by k^n, where $n=1$, 2, or 3 depending on the atomic number of the backscattering atom. This is to compensate for amplitude reduction as a function of k, due in part to the $1/k$ dependence in the EXAFS formula,[27] and in part to the k dependence of the structure factor; a suggested guideline is to take $n=3,2,1$ for $Z \lesssim 36$, $36 \lesssim Z \lesssim 57$, $57 \lesssim Z \lesssim 86$, respectively.[30] To account for the possibility of arsenic clustering in addition to isolated arsenic atoms, the analysis has been carried out for the cases of $n=1$ and $n=3$. Different values have also been tried for the number of sections in the spline and the order of the polynomial; in all cases the resulting EXAFS spectra were qualitatively the same. The curves finally obtained and used in our analysis are given by the dots in Figs. 11(a) and (b) for samples LN and LNV, respectively.

The EXAFS spectrum is then Fourier transformed to real space to permit calculation of the distances from the central arsenic atom to its surrounding neighbors. Figures 11(c) and 11(d) are the Fourier transforms of the LNV

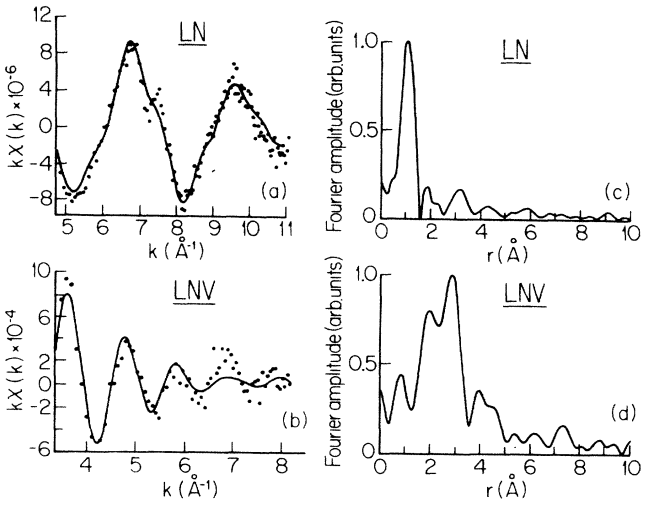

FIG. 11. EXAFS spectra of samples LN and LNV are given by points in (a) and (b), respectively; the solid lines are least-squares fits obtained by back-transforming filtered peaks from the Fourier transforms of the same samples shown in (c) and (d), respectively. See the text for discussion.

TABLE V. Nearest-neighbor distances r_j and shifts in threshold energy ΔE_0 calculated from the EXAFS of samples LNV and LN using the calculated phase shifts of Teo and Lee (Ref. 30).

Sample	Shell (j)	Species	r_j (Å)	ΔE_0 (eV)
LN	a	Bi	1.067±0.017	3.45
	1	As	2.269±0.013	−11.64
	2	Bi	3.326±0.053	−12.82
LNV	a	Bi	1.133±0.012	−1.451
	1	As	2.128±0.012	−6.216
	1	Bi	2.821±0.038	0.320
	2	Bi	3.444±0.048	12.469

[a]Distance calculated is too small to be considered an interatomic distance.

and LN EXAFS, respectively. The positions of the peaks give the relative distances of the neighbors for the two samples. Absolute distances can be extracted once the sum of the central atom and backscattering phase shifts are known, either by calculation or by comparison to a model compound with the same components and known neighbor distances. Due to the extremely low solubility of arsenic in bismuth, no suitable single-crystal alloy samples were available,[31] so distances were extracted using theoretical phase functions interpolated and extrapolated from the tables of Teo and Lee.[30] The results of back-transforming filtered peaks in the Fourier spectrum, allowing the threshold energy E_0 to vary, are given in Table V. Calculations were made allowing for both arsenic and bismuth neighbors by using different backscattering phase shifts; these are specified in the table. For purposes of comparison, the neighbor distances in the pristine bismuth and arsenic lattices are given in Table VI.[32]

At this point, we merely point out that the distance corresponding to the very strong peak in the LN sample and the smaller peak at approximately the same position in the LNV sample is much shorter than any distance that can exist in the arsenic-implanted system. These peaks are certainly real; in the LN sample it is the most prominent feature and the low-frequency oscillations in the EXAFS that give rise to it are clearly visible. Changing k weighting and the length of the spectrum analyzed have no effect on its position or strength relative to the other feature in the spectrum. Possible explanations for this peak are discussed at the end of this section.

Although more quantitative information is derived from a back transform of both the phase and amplitude functions to be fit to the EXAFS spectra, much can be learned from the phase function alone. Looking at the different distances obtained for the two samples, we find that in the LNV sample the As-Bi distances fall between the As-As and Bi-Bi pristine crystal nearest- and next-nearest-neighbor distances. This indicates that the arsenic atoms are at substitutional sites, causing the lattice to contract slightly around them because they are considerably smaller than the bismuth atoms. In the case of sample LN, none of the distances correspond to bismuth crystalline distances, thereby providing evidence that the atoms have found interstitial positions in the lattice. The As-As distance obtained in LNV is somewhat smaller than the arsenic lattice nearest-neighbor distance, so it seems that no precipitation of arsenic occurs and that this peak, which is not completely separated from the strongest peak in the transform, should not be resolved separately.

TABLE VI. Distances (in Å) between neighboring atoms in the virgin bismuth and arsenic lattices (Ref. 32).

Shell (j)	Bismuth	Arsenic
1	3.09	2.68
2	3.59	3.12
3	4.74	4.12

The final step in analysis of the EXAFS data is to back transform the filtered data of the two most prominent peaks and fit them to the k normalized spectrum, allowing some combination of the eight parameters, one each per shell of the jth neighbor distance, r_j, the number of atoms in the jth shell, N_j, a Debye-Waller-type correction for thermal vibrations σ^2, and the threshold energy E_0 to vary. Because the first and last of these parameters influence the oscillation frequency while the second and third determine the amplitude, they are varied in pairs. Since E_0 was allowed to vary to determine a value for r_j, initially these are held fixed and the amplitude parameters are permitted to vary first. Then, using these values, a best fit is obtained for the neighbor distances and threshold energies. The fits for both samples are the smooth curves in Figs. 11(a) and 11(b) and the results of the analysis are summarized in Table VII.

The parameters obtained for the LNV sample are the easier of the two sets to interpret. We find that an arsenic atom has three nearest and three next-nearest-neighbor bismuth atoms, the same as an atom in the pristine bismuth lattice. The neighbor distances lie between the values for the pristine bismuth and arsenic lattices as would be expected for an arsenic atom at a substitutional site in the bismuth lattice. We conclude, therefore, that for implantation at warmer temperatures, atoms come to rest at substitutional sites, with some lattice relaxation occurring. The parameters obtained for the LN sample are more difficult to interpret. Because the peak at the anomalously small-r value is the strongest feature in the Fourier transform, it must be included in any further analysis of the data. Since this distance cannot be physically interpreted as a distance to the central arsenic atom, the other parameters also are in question. However, we do obtain a reasonable fit and include these results as well.

TABLE VII. Results of two-shell fitting of the EXAFS data, considering the largest peak in each Fourier transform as the actual first shell.

Sample	Shell	r_j	N_j	ΔE_0 (eV)	σ^2 (Å^2)
LN	1	1.061	1	0.40	−0.000 31
	2	3.364	1	5.844	−0.000 29
LNV	1	2.891	3	−0.43	0.0450
	2	3.364	3	13.44	0.0043

The results of our EXAFS data support the suggestion that heating of the sample by the ion-beam current during implantation is sufficient to anneal point defects, even when the sample is cooled with dry ice during implantation, allowing the implanted atoms to come to rest in substitutional sites. When this effect is suppressed by cooling the sample to very low temperatures during implantation, ions appear to come to rest at interstitial positions. As seen in Sec. III, regardless of sample temperature during implantation, the introduction of foreign species to the lattice causes long-range strains which affect the electronic energy structure.

IV. RUTHERFORD-BACKSCATTERING CHANNELING MEASUREMENTS

An experiment that provides data complementary to that obtained from EXAFS measurements on the damage induced in the lattice is Rutherford-backscattering spectrometry (RBS) channeling. In this experiment, MeV He ions are directed along a high symmetry axis of the crystal. At these energies, the particle wavelengths are of the order of 10^{-12} cm so that the lattice is viewed as a real crystal of rows of atoms that steer the beam via Coulombic interactions, allowing the ions to penetrate deeply into the sample.[33] These channeled particles can be scattered to nonchanneling trajectories (i.e., dechanneling) as they penetrate into the crystal. In a perfect crystal, the ions are dechanneled due to both multiple scattering by electrons and collisions with thermally displaced atoms. The presence of defects in a crystal gives rise to additional effects.

(i) Atoms blocking the channel can cause close-encounter wide-angle collisions leading to the direct detection of the backscattered probing particles.

(ii) Small-angle forward-scattering collisions can lead to dechanneling if the incident particles are deflected at angles greater than the critical angle for channeling.

(iii) Extended defects can cause distortion or curvature of the channel wall, resulting in a greater dechanneling effect than thermal vibrations.

These effects cause distinctive features in the backscattered yield $\chi(E)$; direct scattering of the particles results in a bump (called the damage peak) in the backscattered spectrum, while extended defects cause an increase in the slope $d\chi/dE$.[33] Since the depth at which the He ions are backscattered is related to their energy upon detection, RBS-channeling analysis also permits determination of the region where the lattice is damaged or distorted.

A. Experimental results

The channeling experiments were done on two similar facilities, one at AT&T Bell Laboratories[34] and the other at Cornell University[35] using $^4He^+$ ions in the 2- to 3-MeV energy range. The experimental setup is described in detail elsewhere.[20] The samples used were the same as those in Sec. III. Preliminary results of the channeling experiments on ion-implanted bismuth were reported earlier.[4] In the more complete discussion that follows, all calculations utilize the yields normalized to the random signal.

The results of channeling 2-MeV $^4He^+$ ions along the binary axis of bismuth are seen in the bottom spectrum in Fig. 12(a). Several features of this spectrum indicate the good crystallinity of our sample, cut from the same crystal as most of the implanted samples. First, at the high-energy end there is a sharp peak due to direct scattering from the surface layer atoms. Because these atoms are in good alignment with the succeeding layers, the yield falls rapidly to its minimum value, only 0.054 times the corresponding yield for the unaligned crystal. This compares favorably with the ratio of 0.045 typically obtained in silicon crystals aligned along the (100) axis. The very small change in the aligned yield over approximately 150 channels, corresponding to $d\chi/dE \sim 0.7$ MeV^{-1}, is also reflective of the good crystal quality of the sample.

Also seen in Fig. 12(a), is the RBS spectrum from sample $\mathscr{A}$ cooled with icewater during implantation with 200-keV arsenic ions to a fluence of 5.0×10^{16} cm^{-2}. Several features in the implanted aligned spectrum of Fig. 12(a) are worthy of note. First, the surface peak is still discernible, which means that there is only a small amount of damage in the region close to the surface, consistent with the assumptions made in Sec. II. The yield does not fall to as small a value as in the virgin crystal; in this case $\chi \simeq 0.13$ immediately below the surface peak, and increases at a much greater rate as we move away from the surface. Using the calibration of 4 keV per channel, the slope $(d\chi/dE)$ is ≈ 0.76 MeV^{-1} up until about 400 channel numbers [see Fig. 12(a)] which is equivalent to a depth of about 3200 Å according to the energy to depth conversion scale of Ziegler and Chu;[36] this represents the strained volume of the crystal. This change in slope $(d\chi/dE)$ can be explained by the same model used to calculate the strain in Sec. IV B of this paper; bismuth atoms are displaced by implanted arsenic atoms assuming substitutional sites, creating dislocation lines, and straining the lattice. At some depth, $\sim$3000 Å, the dislocation lines end and the effect of the implanted arsenic is manifest

merely as strains in the lattice. The presence of the bend in the RBS spectrum (at ~340 channel number) is similar to the spectrum obtained in implanted HgCdTe by Bahir *et al.*,[37] who also explained their results in terms of long-range strains in the crystal.

Figure 12(b) is the backscattered yield from sample $\mathscr{B}$, cooled with dry ice and isopropyl alcohol during the implantation of arsenic to a total fluence of 5.0×10^{16} cm^{-2} using the three energies 40, 100, and 200 keV. This RBS aligned spectrum shows evidence for greater amounts of the same type of damage observed in the sample cooled with icewater during implantation. The backscattered yield is much greater at all depths due to the presence of more defects in the lattice. At its minimum value, the normalized yield is 0.34. In the region closest to the surface extending to a depth of ~870 Å, a rounded damage peak is clearly visible. This depth correlates very closely with the LSS theoretically predicted arsenic profile for this sample which drops off at approximately 1000 Å indicating that the peak is caused by backscattering from bismuth atoms that have been further displaced than in sample $\mathscr{A}$.

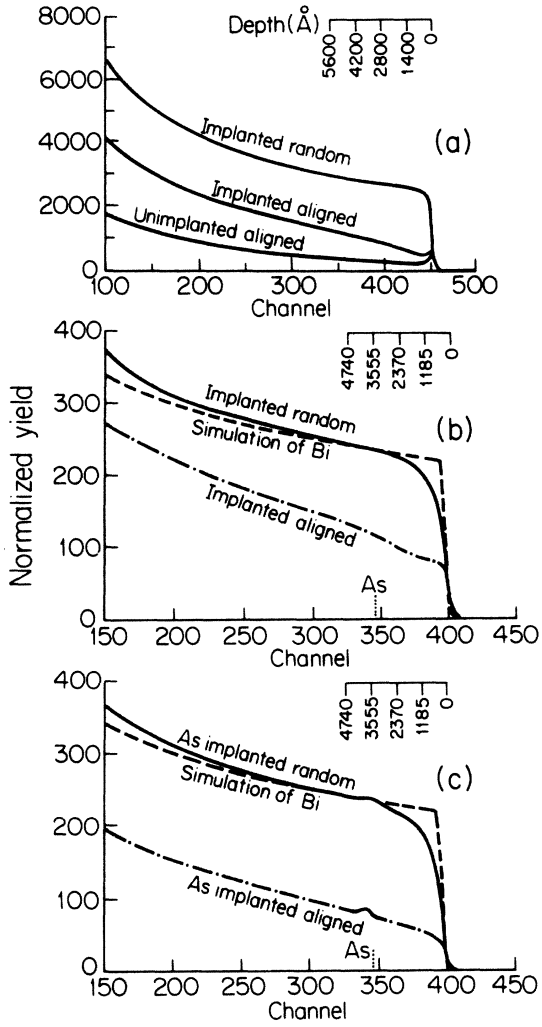

FIG. 12. Energy spectra for 2-MeV He ions backscattered from unimplanted and implanted bismuth samples in random and aligned (along the binary axis) geometries. Samples were all cooled during implantation with 200-keV As ions to fluence 5.5×10^{15} cm^{-2}. Coolants used for the different samples were (a) icewater, (b) dry ice and isopropyl alcohol, and (c) liquid N_2. The depth scales from the sample surface are given for each sample. For samples (b) and (c) the energy (on the channel number scale) of a He ion backscattered from an arsenic atom on the sample surface is indicated.

The knee structure is again obtained in Fig. 12(b), but is much more pronounced. In this sample, the initial slope $d\chi/dE$ is 0.81 MeV^{-1}, slightly higher than the value in the sample cooled with icewater during implantation. This increase may be due to the presence of more line defects than in sample $\mathscr{A}$. The discontinuity in slope occurs at roughly the same depth as in sample $\mathscr{A}$, providing further support for the model above: that bismuth atoms are displaced in the lattice out to approximately 1000 Å, beyond which atoms are sufficiently close to their "normal" positions to be described by a strain model. Thus, the damage introduced into the bismuth lattice cooled with dry ice during implantation consists of displaced Bi atoms in the first 1000 Å below the surface and of dislocations and vacancies through the implanted region and beyond for an additional ~2000 Å.

The aligned backscattered yield from sample $\mathscr{C}$, cooled with liquid nitrogen during implantation is seen in Fig. 12(c) to be qualitatively different from the spectra of the two implanted samples discussed above. Surprisingly, the yield from sample $\mathscr{C}$ is noticeably lower than that from sample $\mathscr{B}$; just beyond the surface, the normalized yield is 0.31. This can perhaps be explained if the crystallinity of this sample was somewhat better initially than that of sample $\mathscr{B}$. Before implantation, diffractometer scans were taken from all samples to test their crystallinity and orientation; the $(1\bar{1}0)$ Bragg peak for sample $\mathscr{C}$ was about 1.2 times stronger than the sample $\mathscr{B}$ peak; the corresponding ratio of the normalized RBS-channeling yields is 1.1.

There is no surface peak observed in sample $\mathscr{C}$, indicating an increased amount of surface damage. The most distinctive feature of this spectrum, however, is the presence of a direct scattering peak corresponding to backscattering from the arsenic implants. This can only be due to a significant number of arsenic atoms blocking the channels, as noted above. Integration to calculate the area under this peak gives the fluence of implanted ions; a computer calculation results in 5.0×10^{16} cm^{-2}, the fluence to which this sample was implanted, thus supporting the interpretation that all the arsenic ions are at interstitial sites in the lattice for the liquid nitrogen cooled sample.

Information on the profile of the interstitials is obtained from the width of the peak. The energy obtained is converted to a length using the arsenic energy to length conversion from the work of Ziegler and Chu.[36] This gives $R_p+\Delta R_p\simeq1080$ Å which is very close to the 917-Å value predicted by LSS theory. This, too, helps to identify the peak as due to arsenic interstitials. The RBS result corroborates the evidence obtained from the EXAFS data on this sample that the arsenic atoms are at interstitial positions in the lattice, possibly in clusters.

TABLE VIII. Summary of RBS-channeling results.

Coolant	Feature(s)	Significance
Icewater (~273 K)	Discontinuity in slope at 3200 Å	Extended defects to ~3200 Å
Dry ice-alcohol	Direct Bi defect scattering from surface to an 870-Å depth	Bismuth interstitials in implanted region
(~217 K)	Discontinuity in slope at 3000 Å	Extended defects to 3000 Å
Liquid Nitrogen	Direct arsenic scattering peak	Arsenic interstitials in implanted region from surface to 1080 Å
(~77 K)	Slope of RBS yield is approximately constant but greater than pristine bismuth slope	Long-range scattering throughout sample

B. Conclusions

These RBS-channeling experiments give complementary information concerning damage to the bismuth lattice caused by arsenic implantation. We find that the damage increases for decreased implantation temperature, consistent with the results of the magnetoreflection measurements. In addition, there is evidence that at the lowest implantation temperatures, arsenic ions come to rest at interstitial positions in the lattice, while at temperatures greater than about −50 °C the implanted ions find substitutional sites. This is consistent with data obtained from EXAFS spectra. For samples implanted at higher temperatures, a discontinuity in $d\chi/dE$ is observed similar to that seen in implanted HgCdTe (Ref. 37) and aluminum,[38] indicating the presence of extended defects and strains in the lattice. The results of Sec. IV are summarized in Tables VIII and IX.

V. DISCUSSION

In this section we use the results of the EXAFS and RBS-channeling experiments to explain the change in electronic band parameters obtained from the magnetoreflection measurements in terms of changes to the bismuth lattice. Referring again to Fig. 7, we note the decrease in the L-point energy gap as a function of fluence and size of the implanted atoms. Previous magnetoreflection studies of bismuth found that the energy gap increases upon application of hydrostatic pressure.[39] In that work, Mendez found that the hydrostatic shifts could be fit by deformation potential theory[17,40] using Walther's parameters.[41] Since the presence of atoms physically introduced into the lattice are expected to stretch the lattice from within, we use the following strain model derived from the work of Eshelby.[42] The implanted ion is taken to be a sphere forced into a spherical hole of slightly different size in an infinite block of elastic material; this model holds for both interstitial and substitutional impurities. In the absence of external forces, the displacement vector $\mathbf{u}$ must satisfy the differential equation

$$\mu\nabla^2\mathbf{u}+(\lambda+\mu)\nabla\times\nabla\cdot\mathbf{u}=\mathbf{0} \tag{7}$$

in which λ and μ are the coefficient of compressibility and shear modulus, respectively. Away from the defect, the strain field $\mathbf{u}^\infty$ must be spherically symmetric and must not increase with distance. The only solution of Eq. (7) which satisfies these requirements is

$$\mathbf{u}^\infty=-c\nabla\left[\frac{1}{r}\right], \tag{8}$$

where the constant c measures the strength of the defect distortion and is taken to be the defect volume. When a defect is introduced at any point within a closed surface Σ_0 in the infinite crystal, a surface element dS with normal $\mathbf{n}$ sweeps out a volume $\mathbf{u}^\infty\cdot\mathbf{n}dS$. For the case of an impurity atom introduced by ion implantation, expansion is allowed only orthogonal to the direction of implantation, so the "volume" enclosed by Σ_0 becomes an area and increases by

$$\Delta V^\infty=\int_{\Sigma_0}\mathbf{u}^\infty\cdot\mathbf{n}\,dS=c\int_{\Sigma_0}\frac{\mathbf{r}\cdot\mathbf{n}}{r^3}dS=\frac{2\pi c}{R_I}, \tag{9}$$

where R_I is the radius of the implant. For Σ_0 to be a free surface, an image displacement u^I produced by surface tractions $\mathbf{T}$ over Σ_0, must be added to $\mathbf{u}^\infty$. The additional image volume is given by

TABLE IX. Comparison for different implantation temperatures of the minimum yield $\chi_{\min}$ and the derivative $d\chi/dE$ for the first 3000 Å from the surface.

Implantation coolant	$\chi_{\min}$	$d\chi/dE$ MeV^{-1}
Icewater (~273 K)	13%	0.757
Dry ice (~217 K)	34%	0.806
Liquid N_2 (~77 K)	31%	0.419

TABLE X. Calculated trigonal strain ϵ_3 for bismuth implanted with 150-keV ions to the various fluences studied by the magnetoreflection experiment. R_I is the radius of the implanted ion and ΔR_p is the width of the implanted region.

Ion	R_I (Å)	ΔR_p (Å)	Fluence ($\times 10^{15}$ cm^{-2})	ϵ_3
As	1.18	289	2.2	0.0034
			5.5	0.0046
			10.0	0.0056
Sb	1.36	221	5.5	0.0051
Bi	1.44	154	2.2	0.0042
			5.5	0.0057

$$\Delta V^I=\frac{1}{3K}\int \mathbf{r}\cdot\mathbf{T}\,dS=-\frac{2\mu}{3K}\int_{\Sigma_0} x_i\frac{\partial}{\partial x_i}u_k^{\infty}\,dS_k\ , \quad (10)$$

where K is the bulk modulus of the crystal. Since u_k^{∞} is homogeneous of degree -2, the integral in Eq. (10) is -2 times that in Eq. (9) and

$$\Delta V^I=\frac{2\pi c}{R_I}\left[\frac{4\mu}{3K}\right] \quad (11)$$

so that the total areal change is

$$\Delta V^T=\frac{2\pi c}{R_I}\left[1+\frac{4\mu}{3K}\right]\equiv\frac{2\pi c\gamma}{R_I}\ . \quad (12)$$

A density of defects n, causes a uniform dilation between defects given by

$$\frac{\Delta V}{V}=\frac{2\pi c(\gamma-1)n}{R_I}\ . \quad (13)$$

For a crystal like bismuth whose symmetry deviates only slightly from cubic symmetry, $\gamma=K/c_{11}^0$, where the bulk modulus K is approximately given by the cubic value of $c_{11}+2c_{12}$ and

$$c_{11}^0=\tfrac{3}{5}(c_{11}+2c_{12}+4c_{44}) \quad (14)$$

is an average elastic constant value. The c_{ij} are taken from Epstein and deBretteville.[43] At room temperature, in units of 10^{10} dyne cm^{-2}, $c_{11}=62.90$, $c_{12}=35.10$, and $c_{44}=10.84$, so that

$$\gamma=1.33\ . \quad (15)$$

Finally, we need to compensate for the anisotropy of the in-plane expansion. The bulk compressibility constant in the trigonal direction is 2.83 times that in the perpendicular directions so that

$$\epsilon_3=\frac{\Delta c}{c}=0.15\frac{\Delta V}{V}\ . \quad (16)$$

The number density of implants is calculated from LSS theory:[19]

$$n=\frac{\phi}{2\Delta R_p} \quad (17)$$

so that the final expression for the trigonal expansion is

$$\epsilon_3=0.15(\gamma-1)n^{2/3}R_I^2=0.05\left[\frac{\phi}{2\Delta R_p}\right]^{2/3}R_I^2\ . \quad (18)$$

In the above derivation, the lattice strain is caused by the presence of interstitial impurity atoms. The EXAFS and RBS-channeling results show, however, that for samples implanted at room temperature, the implanted atoms rest at substitutional sites, displacing bismuth atoms which then come to rest at interstitial sites deeper in the sample. In all cases, then, the lattice strain is caused by bismuth interstitials; the different strain manifest in samples implanted with different atomic species is due to a contraction of the lattice around the smaller substitutional atom, proportional to the ratio of the volume of the implanted atom to that of bismuth. The pertinent radii and resulting strains are given in Table X.

In the deformation potential model, the energy bands are each shifted an amount proportional to the strain. Using the deformation potential values $D_{22}=-5.9$ eV and $D_{33}=1.71$ eV,[41] we obtain the following relation between strain in the trigonal direction, ϵ_3 and change of E_g:

$$-\Delta E_g=0.74\epsilon_3\ \text{meV}\ . \quad (19)$$

Figure 13 is a plot of this line and data points from our magnetoreflection experiments. We note that the experimental points follow a linear trend and that the deforma-

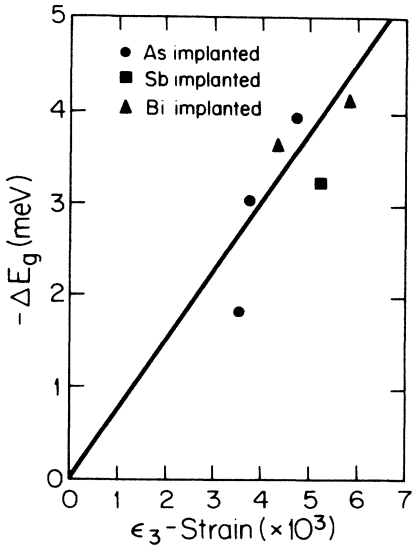

FIG. 13. Fit of the magnetoreflection results for the implantation-induced decrease in band gap to the strain model calculation (see text).

tion potential theory describes the experiment quite well.

To summarize, it has been shown that not only are magnetoreflection experiments possible in ion-implanted bismuth, but that the spectra are sufficiently like those of pristine bismuth to permit their analysis in terms of the basic bismuth band model with modified band parameters and some breakdown in selection rules. Specifically, the small band gap at the L point becomes yet smaller for increased fluence and size of implanted species, and the effective mass along the binary direction at the L point also decreases as a function of these quantities in such a manner that $\gamma \sim E_g/m^*$ increases. Using deformation potential theory, the effect of implantation on E_g is shown to be due to strains in the lattice.

Magnetoreflection measurements also provided much information on the damage induced in the bismuth lattice by the implantation process. Because of very low melting temperature of bismuth (271.3 °C), it was decided to study samples cooled to different temperatures during implantation to determine if any annealing occurs during room-temperature implantation. At lower implantation temperatures, broadened linewidths are observed, as well as forbidden transitions which indicate breaking of the inversion symmetry of lattice. For low beam current implantation at low temperature, impurity-level transitions very much like those seen in the $Bi_{1-x}Sn_x$ alloy magnetoreflection spectra are observed.

Experiments giving a more direct measure of the structural changes were also carried out; specifically (EXAFS) extended x-ray-absorption fine structure and Rutherford-backscattering (RBS) channeling measurements. These corroborate the picture developed from the magnetoreflection measurements that when the sample is at $\gtrsim 50$ °C, implanted atoms occupy substitutional sites while for lower temperatures implanted species are at interstitial positions. The channeling measurements showed the presence of long-range strain in all samples and exhibited direct scattering from implants at interstitial positions for samples cooled with liquid nitrogen during implantation.

ACKNOWLEDGMENTS

We gratefully acknowledge the following people for assistance with the various experiments: Dr. B. S. Elman, A. Antonious, and Dr. G. Braunstein with magnetoreflection, Dr. A. I. Goldman, E. Canova and S. Woronick with EXAFS, and Drs. G. Galvin and G. Braunstein with RBS channeling. We also express our gratitude to the staffs of the Francis Bitter National Magnet Laboratory and the Cornell High Energy Synchrotron Source (CHESS) for technical assistance, especially Dr. B. Brandt and Dr. R. Aggarwal of the Magnet Laboratory. Several people helped with the implantation samples, M. Rothman formerly of the Materials Research Center at the Massachusetts Institute of Technology (MIT) and M. Skvarla of the National Research and Resource Facility for Submicron Structures at Cornell University. We would also like to thank two staff members of AT&T Bell Laboratories, J. Garno for lessons in bismuth electropolishing, and B. Kincaid for the use of his EXAFS analysis programs and many long helpful discussions on their use and on analysis of the EXAFS data. Finally, we acknowledge Dr. G. S. Cargill III, Dr. A. Erbil, Dr. G. Dresselhaus, Dr. G. Braunstein, D. Gabbe, and J. Alexander for helpful and stimulating discussions on many aspects of this work.

*Present address: Department of Physics, Ben-Gurion University of the Negev, P.O. Box 653, 84 120 Be'er Sheva, Israel.

[1]J. W. Mayer, L. Eriksson, and J. A. Davis, *Ion Implantation in Semiconductors* (Academic, New York, 1970).

[2]E. M. Kunoff, B. S. Elman, and M. S. Dresselhaus, *Ion Implantation and Ion Beam Processing of Materials* (North-Holland, New York, 1983), p. 553.

[3]B. S. Elman, L. McNeil, C. Nicolini, T. C. Chieu, M. S. Dresselhaus, and G. Dresselhaus, Phys. Rev. B **28**, 7201 (1983).

[4]E. M. Kunoff, M. S. Dresselhaus, and Y. H. Kao, in *Advanced Photon and Particle Techniques for the Characterization of Defects in Solids* edited by J. B. Roberto, R. W. Carpenter, and M. C. Wittel (North-Holland, New York, 1984), Vol. 41, p. 281.

[5]R. N. Brown, J. G. Mavroides, and B. Lax, Phys. Rev. **129**, 2055 (1963).

[6]G. E. Smith, G. A. Baraff, and J. M. Rowell, Phys. Rev. **135**, A1118 (1964).

[7]H. T. Chu and Y. Kao, Phys. Rev. B **1**, 2369 (1970).

[8]M. P. Vecchi, J. R. Pereira, and M. S. Dresselhaus, Phys. Rev. B **14**, 298 (1976).

[9]M. H. Cohen, L. M. Falicov, S. Golin, IBM J. Res. & Dev. **8**, 215 (1964).

[10]P. A. Wolff, J. Phys. Chem. Solids **25**, 1057 (1964).

[11]A. A. Abrikosov and L. A. Falcovskiĭ, Zh. Eksp. Teor. Fiz. **43**, 1089 (1962) [Sov. Phys. JETP **16**, 769 (1963)].

[12]C. Nicolini, T. C. Chieu, G. Dresselhaus, and M. S. Dresselhaus, Solid State Commun. **43**, 233 (1982).

[13]M. P. Vecchi, Ph.D. thesis, Massachusetts Institute of Technology, 1975 (unpublished).

[14]M. S. Maltz, Ph.D. thesis, Massachusetts Institute of Technology, 1968 (unpublished).

[15]M. Maltz and M. S. Dresselhaus, Phys. Rev. B **2**, 2877 (1970).

[16]M. P. Vecchi and M. S. Dresselhaus, Phys. Rev. B **9**, 3257 (1974).

[17]E. E. Mendez, A. Misu, and M. S. Dresselhaus, Phys. Rev. B **24**, 639 (1981).

[18]A. Misu, T. C. Chieu, M. S. Dresselhaus, and J. Heremans, Phys. Rev. B **25**, 6155 (1982).

[19]J. Lindhard, M. Scharff, and H. E. Schiøtt, K. Dan. Vidensk. Selsk., Mat. Fys. Medd. **33**, 14 (1963).

[20]E. M. Kunoff, Ph.D. thesis, Massachusetts Institute of Technology, 1985 (unpublished).

[21]G. A. Baraff, Phys. Rev. **137**, A842 (1964).

[22]W. S. Boyle and A. D. Brailsford, Phys. Rev. **120**, 1943 (1960).

[23]S. Golin, Phys. Rev. **166**, 643 (1968).

[24]P. R. Schroeder, Ph.D. thesis, Massachusetts Institute of Technology, 1969 (unpublished).

[25]G. Dearnaley, J. H. Freeman, R. S. Nelson, and J. Stephen, *Ion Implantation* (American Elsevier, New York, 1973).

[26]J. M. Ziman, *Principles of the Theory of Solids* (Cambridge University, New York, 1979).

[27]P. A. Lee, P. H. Citrin, P. Eisenberger, and B. M. Kincaid, Rev. Mod. Phys. **53**, 769 (1981).

[28]A. H. Erbil, G. S. Cargill III, and R. F. Boehme, in *Advanced Photon and Particle Techniques for the Characterization of Defects in Solids,* edited by J. B. Roberto, R. W. Carpenter, and M. C. Wittels (North-Holland, New York, 1984), Vol. 41, p. 275.

[29]E. A. Stern and S. M. Heald, Rev. Sci. Inst. **50**, 1579 (1979).

[30]B. K. Teo and P. A. Lee, J. Am. Chem. Soc. **101**, 2815 (1979).

[31]Acknowledgment is made to Professor G. Saunders of the University of Bath, Great Britain for his efforts to introduce sufficient As concentration into Bi for use as a standard reference.

[32]A. I. Goldman (unpublished).

[33]L. C. Feldman, J. W. Mayer, and S. T. Picraux, *Materials Analysis by Ion Channeling* (Academic, New York, 1982).

[34]Measurements kindly carried out by Dr. G. Braunstein.

[35]Measurements kindly carried out by Dr. G. Galvin.

[36]J. F. Ziegler and W. K. Chu, At. Data Nucl. Data Tables **13**, 463 (1974).

[37]G. Bahir, T. Bernstein, and R. Kalish, Radiat. Eff. **48**, 247 (1980).

[38]M. K. Agrawal and D. K. Sood, Nucl. Instrum. Methods **149**, 425 (1978).

[39]E. E. Mendez, Ph.D. thesis, Massachusetts Institute of Technology, 1979 (unpublished).

[40]J. Bardeen and W. Shockley, Phys. Rev. **80**, 72 (1950).

[41]K. Walther, Phys. Rev. **174**, 782 (1968).

[42]J. D. Eshelby, Solid State Phys. **3**, 79 (1956).

[43]S. Epstein and A. P. deBretteville, Jr., Phys. Rev. **138**, A771 (1965).